Theoret. Chim. Acta (Berl.) 56, 113–123 (1980)

THEORETICA CHIMICA ACTA

Binding/Antibinding Analyses for Diatomic Interactions. The HeH^{2+} System

Toshikatsu Koga and Mutsuo Morita

Department of Industrial Chemistry, Muroran Institute of Technology, Muroran, 050 Japan

On the basis of the Berlin diagram, the region-functional contribution of the electron density has been quantitatively examined for the $1s\sigma$, $2p\sigma$, and $2p\pi$ states of HeH^{2+} system. The binding and antibinding contributions and the dynamic behaviours of the electron density during the interaction processes are discussed in comparison with the previous results for homonuclear H_2^+ system. The effect of coordinate-dependence of the Berlin diagram on the regional partitioning has also been studied.

Key words: Berlin diagram – Hellmann – Feynman force – HeH^{2+} system.

1. Introduction

The Berlin diagram [1] which regionally divides the distribution of the diatomic electron density into binding and antibinding parts provides a unique interpretation for the role of the electron density in chemical bonding from the viewpoint of the electrostatic Hellmann–Feynman (H–F) theorem [2–4]. Recently, a generalization of such region-functional concept of the electron density has been also proposed for polyatomic systems (generalized Berlin diagram) [5]. These diagrams have been *qualitatively* but successfully used to interpret the dynamic behaviour of the electron density in nuclear rearrangement processes such as molecular geometries, chemical reactions, and long-range forces [3–10].

In a previous paper [11], we have *quantitatively* examined the regional contribution of the electron density for the four low-lying electronic states of H_2^+ system. Using the exact analytical wavefunctions of the system, the electronic charge, H–F force, and stabilization energy have been partitioned into the binding and antibinding components, and their roles in the attractive/repulsive and σ/π-type interaction processes have been analysed in detail. The center of electron density (CED) and the center of force density (CFD) have been also used to clarify the dynamic behaviour of the electron density.

A purpose of the present article is to extend the quantification of the regional

0040-5744/80/0056/0113/$02.20

concept of Berlin diagram to heteronuclear diatomic systems. We have chosen the one-electron system HeH^{2+} for which the exact wavefunctions are known [12–14]. Since H_2^+ and HeH^{2+} are prototypes of homo- and heteronuclear diatomics, it may deserve some interest to compare the results of the binding/antibinding analyses for these two systems based on the exact wavefunctions. It is also a purpose of this study to investigate the effect of the coordinate-dependence of the regional partitioning which appears for heteronuclear systems. We have examined two different partitionings which result from the Berlin diagrams in the GCN (geometric-center-of-the-nuclei) and CMN (center-of-mass-of-the-nuclei) coordinates [5]. In the next section, the computational method is briefly given and the coordinate-dependence of the partitioning is discussed in Sec. 3. Then the binding/antibinding analyses are given for the three low-lying $1s\sigma$, $2p\sigma$, and $2p\pi$ states, and the results are compared with those of the homonuclear H_2^+ system.

2. Computational Method

The contribution of the electron density to the diatomic interaction is regionally distinguished into the binding and antibinding parts by the Berlin diagram (see e.g., Fig. 1) [1, 5]. Then, the electronic charge and the H–F force are partitioned into binding and antibinding contributions by the regional integrations as described in a previous paper [11]. The integration of the partitioned forces with respect to the internuclear distance (R) gives the partitioned stabilization energies. These energies are characterized by their direct relationship with the behaviour of electron density (compare with the traditional energetic interpretation (see e.g. [15])).

The CED (center of electron density) and its components have been defined similarly to the previous case [11] on the basis of the atomic region proposed by Politzer [16]. In order to obtain a single index for the system, we have averaged two atomic CED's using the corresponding electronic charges as weighting factors. Though the component CED's depend on the Berlin diagram employed (see later), the total CED is independent of it by the definition. The CFD (center of force density) and its components have been analogously

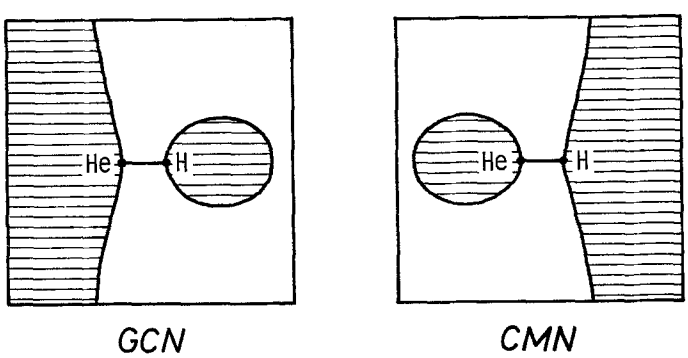

Fig. 1. The Berlin diagrams in the GCN and CMN coordinates. The antibinding regions are shaded

calculated, but they have not been given here since the behaviours of the CED's and CFD's have been almost parallel as they were in H_2^+ system [11].

The wavefunctions have been taken from Ref. [12] for $0.5 \leq R \leq 5.0$a.u. For 5.0a.u. $< R$, we have derived them from the eigen-parameters reported in Refs. [13, 14].

3. Coordinate-Dependence of Regional Partitioning

Since the expression of the force operator is coordinate-dependent, the Berlin diagram also depends on the choice of the coordinate system [5]. We here examine two regional partitionings using the Berlin diagrams in the GCN and CMN coordinates. The former was originally derived by Berlin and there the boundary surfaces of the binding and antibinding regions are determined by the ratio of the nuclear charges [1]. On the other hand, the latter has been introduced to exclude the external translational motion of the system and hence the boundary surfaces depend on both the masses and charges [5]. As shown in Fig. 1, the two Berlin diagrams for HeH^{2+} system are quite different and just the reverse of each other. We note however that the two boundary surfaces (Fig. 1) are rather similar in the region near the nuclei, where the electron density will be concentrated.

Using these diagrams, we have examined the partitioning of the force, stabilization energy, binding charge, and CED for the three states of HeH^{2+} system. The results of the calculations are compared in Figs. 2, 5, 7 (force and energy) and Figs. 3, 6, 8 (binding charge and CED). In these figures, we see that the results of the CMN (solid lines) and GCN (dashed lines) partitionings are almost parallel. In a quantitative sense, the differences between the two curves are smaller for the force and energy, while they are larger for the binding charge and CED in the π state. These may be understood from the nature of the π density which delocalizes away from the molecular axis, since the density near the axis and the nuclei contributes more to the force (and then to the energy) whereas the whole density distribution equally does to the binding charge and the CED.

The parallelism of the present results obtained from the different partitionings is interesting. It seems to suggest that some important aspects of the density distribution in molecular systems might be clarified through the present approach of the region-functional analyses. In the following section, we shall discuss the regional role of the electron density during the three interaction processes.

4. Binding/Antibinding Analyses

4.1. $1s\sigma$ *State*

Although the $1s\sigma$ state is the lowest-energy state of the system, no stable molecule is formed; the force and energy are respectively repulsive and destabilizing throughout the process (Fig. 2).

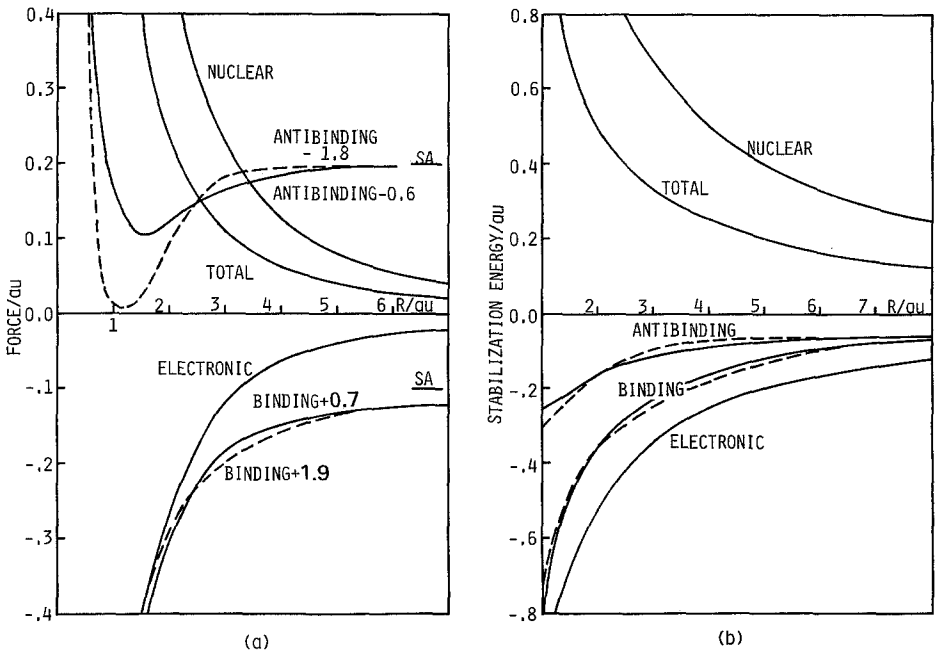

Fig. 2. $1s\sigma$ State. (a) Partitioning of the H–F force. Negative and positive values correspond to attraction and repulsion, respectively. The SA values are $\mp 0.8/\mp 2.0$a.u. (CMN/GCN) for the binding and antibinding forces. (b) Partitioning of the stabilization energy. Negative and positive values correspond to stabilization and destabilization, respectively. The solid lines mean the CMN partitioning, while the dashed lines the GCN one

In Fig. 2a, the binding force monotonously increases its attraction from the separated atom (SA) value. The antibinding force decreases its repulsion for $R \gtrsim 0.8$a.u. with the minimum at $R \simeq 1.6/1.1$a.u. (CMN/GCN). Thus both the binding and antibinding changes are cooperative for attraction (Fig. 2a) and stabilization (Fig. 2b). The results are similar to those of the $1s\sigma_g$ state of H_2^+ system, except for the predominance of the binding part in the present energy curves. However, the nuclear contribution dominates over the electronic one (i.e., the sum of the binding and antibinding contributions), leading to the repulsion of the system (total curves in Fig. 2).

The amount of binding charge (Fig. 3a) shows a monotonous increase as R lowers with a peak at $R \simeq 0.8$a.u. The behaviour again resembles to that found in the $1s\sigma_g$ state of H_2^+ system [11]. However, the net increase from the non-interacting atomic density is small: it is at most $0.04/0.10e^-$ (CMN/GCN). This should be compared with $0.14e^-$ of the stable $1s\sigma_g$ state at $R_e = 2.00$a.u. [11]. The total CED (Fig. 3b) shifts inwardly corresponding to the increase of the binding charge. The maximum shift is 0.05a.u. (at $R \simeq 1.7$a.u.), while it was 0.32a.u. (at $R \simeq 4$a.u.) in the $1s\sigma_g$ state. The binding and antibinding CED's are relatively unchanged for $R > 2$a.u.

In Fig. 4a, the density reorganization along the molecular axis is depicted using

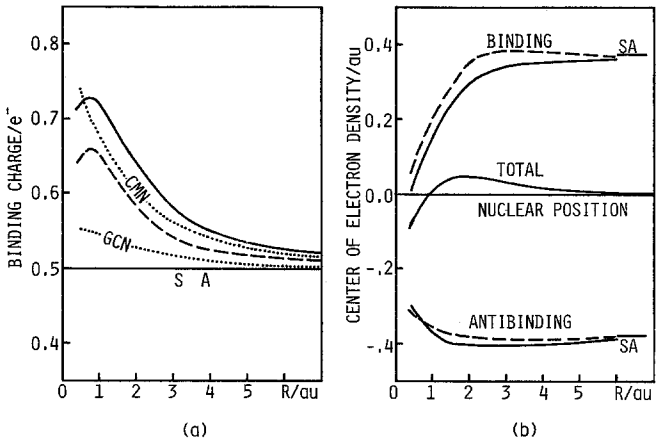

Fig. 3. 1sσ State. (a) Binding charge. The dotted lines show the binding charge obtained from the non-interacting atomic density. The SA value is $0.5e^-$. (b) CED's. Positive value means the inside of the nucleus. The SA values are 0.0, 0.375, and −0.375a.u. for the total, binding, and antibinding CED's, respectively. The solid lines mean the CMN partitioning, while the dashed lines the GCN one

the electron density (ρ) and density difference ($\Delta\rho$). At a large separation ($R \geq 4$a.u.), an inward polarization of the 1s(He) density is observed and this character continues up to R = 1a.u. In shorter distances ($R \leq 3$a.u.), it also leads to the density accumulation in the internuclear region. Therefore the density reorganizations in the binding and antibinding regions result in attraction and

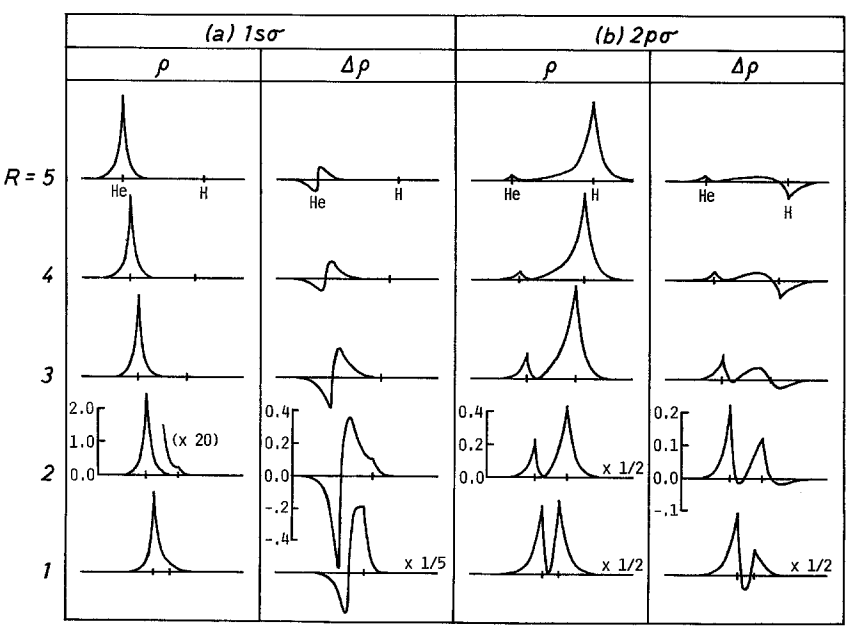

Fig. 4. Electron density ρ and density difference $\Delta\rho$ ($\equiv\rho-\rho_0$) along the internuclear axis. (a) 1sσ State. The reference density ρ_0 has been chosen to ρ_0 = 1s(He). (b) 2pσ State. ρ_0 = 1s(H)

stabilization (electronic part in Fig. 2). For $R \leq 2$a.u., however, the electron density also flows into the antibinding region behind the H nucleus and it works to reduce the attraction of the system.

These density behaviours are the electron-cloud preceding [7] which promotes molecular formation against the nuclear repulsion. However, the present preceding is smaller than that of the $1s\sigma_g$ state as compared through the net binding charge and the shift of the CED. In the present state, appreciable preceding occurs only in shorter R range where the nuclear repulsion is very large. The small preceding may be due to the initial atomic density, 1s(He), which is more tightly bound by the nucleus than 1s(H). In Fig. 4a, we see that the profile of the $1s\sigma$ electron density is very similar to that of the initial 1s(He) density. The electronic charge transferred from the He- to H-atomic region has been calculated to be only $0.06e^-$ even at $R = 2$a.u.

4.2. 2pσ State

In Fig. 5, the partitionings of the force and stabilization energy are given for the $2p\sigma$ state which correlates with 1s(H) in the separated atom limit and with $2p\sigma$(Li) in the united atom limit. The total curves predict a metastable molecule with $R_e \simeq 3.9$a.u. and $\Delta E \simeq 0.0312$a.u. ($\simeq 0.849$eV). In the force curves (Fig. 5a), the origin of this attraction is shown to be the cooperative changes of the two components; the increase of the binding force (maximum

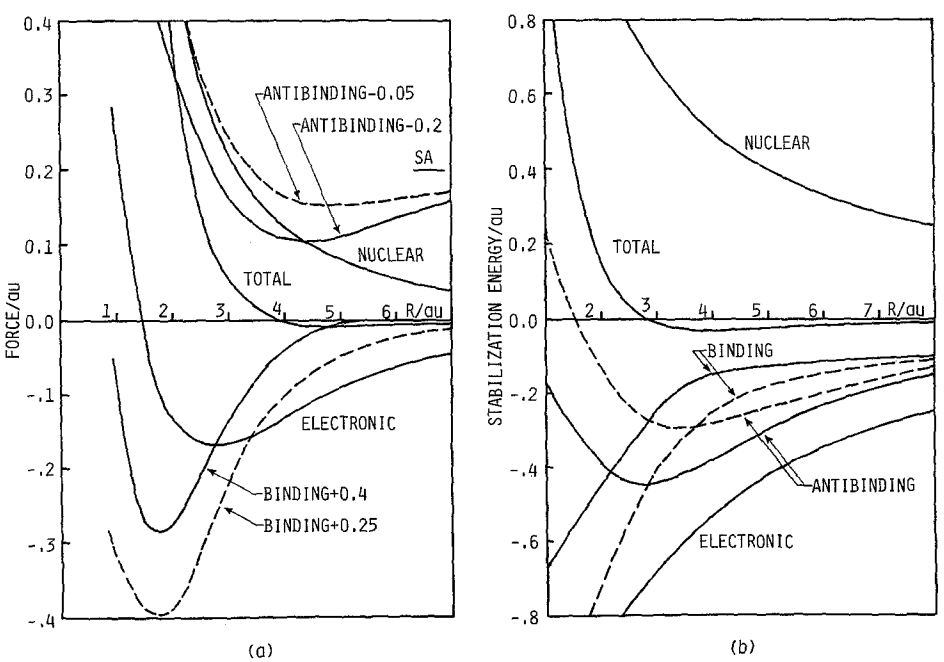

Fig. 5. $2p\sigma$ State. See the captions of Fig. 2. The SA values are now $\mp 0.4/\mp 0.25$a.u. (CMN/GCN) for the binding and antibinding forces

attraction at ~1.8a.u.) and the decrease of the antibinding force (minimum repulsion at ~4.5a.u.). They are also cooperative for the stabilization of the system (Fig. 5b). At $R \simeq 1.4$a.u., the electronic force changes from attractive to repulsive. This is attributed to the $2p\sigma$(Li) character which removes the charge from the binding to the antibinding region (see later). It may be interesting to note that in the energy curves (Fig. 5b) the antibinding contribution is larger than the binding one for $R > 2.2/3.6$a.u. (CMN/GCN). This was also found in the ground state of H_2^+ system, and suggests an important role of the antibinding part especially in σ states.

The density origin of this attraction (and stabilization) is the electron-cloud preceding [7] which appears as the flow of the electron density from the antibinding to the binding region and as the inward shifts of the CED's (Figs. 4b and 6). In Fig. 6a, the binding charge is shown to increase as R decreases with the maximum at $R \simeq R_e$. The net binding charge is also maximum ($0.17/0.14e^-$ (CMN/GCN)) at this distance. The same trend has been seen for the stable $1s\sigma_g$ and $2p\pi_u$ states of H_2^+ [11]. The total CED (Fig. 6b) shifts inwardly for $R > 2$a.u. and the preceding of 0.44a.u. is observed even at R_e. Since there is nodal surface between the nuclei, the electron density (ρ's in Fig. 4b) consists of two "atomic densities". Therefore, the shift of the CED will be related with the degree of the polarization of these densities, i.e., the magnitude of the atomic dipole. The inward and outward shifts of the CED (Fig. 6b) seem to correspond to the attractive and repulsive electronic force (Fig. 5a), respectively. It may also suggest the ionic character of the present attraction, since in the ionic $OH_2 + H^+$ reaction, the atomic dipole (AD) force due to the inward polarization of the atomic density has been shown to dominate over the exchange (EC) force due to the density accumulation in the bond region [18]. The components of the CED first show delocalization and contraction of the

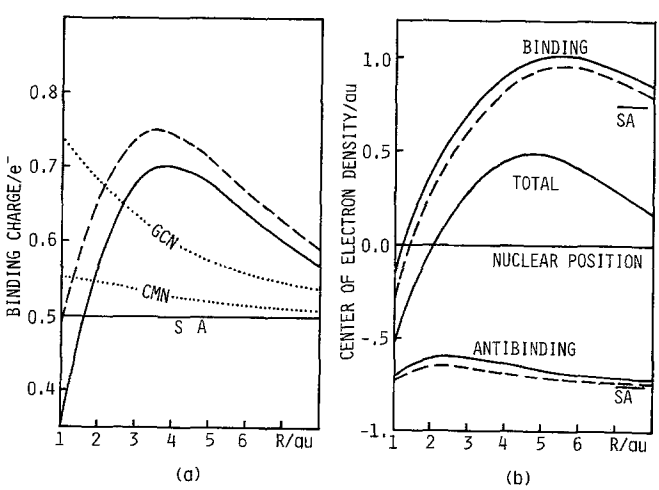

Fig. 6. $2p\sigma$ State. See the captions of Fig. 3. The SA values are now 0.0 and ±0.75a.u. for the CED's

binding and antibinding densities, respectively, and then the opposite reorganizations. The later behaviour is again ascribed to the nodal $2p\sigma$ character. The $\Delta\rho$ figures (Fig. 4b) show that at a large separation (e.g., R = 5a.u.), decrease of the antibinding density behind H and increase of the binding density in the central region of the two nuclei are dominant origin of the attraction, while the density accumulation in the binding region near the nuclei is in a shorter distance (e.g., R = 3a.u.). The initial predominance of the antibinding part is in accordance with the analysis of the stabilization energy as mentioned above. In the intermediate stage, the presence of node makes the binding density distribute near the nuclei, which may be effective to increase the binding force. However, in the later stage, it works to increase the antibinding charge (cf. the binding charge in Fig. 6a) and then the repulsive antibinding force as stated before. Transferability of the loosely-bound 1s(H) density seems important for the attraction in this state, when compared with the 1s(He) density of the repulsive $1s\sigma$ state. In Fig. 4b, the density transfer from the H atom to the binding and He-atomic regions is remarkable even for R = 5a.u. The transferred charge amounts to $0.08e^-$ (at 5a.u.) and $0.10e^-$ (at R_e).

4.3. $2p\pi$ State

The total force and stabilization energy curves (Fig. 7) show no stable bond in this state. Except for the total and nuclear curves, the over-all behaviours of the component forces and energies are similar to those of the attractive $2p\pi_u$ state

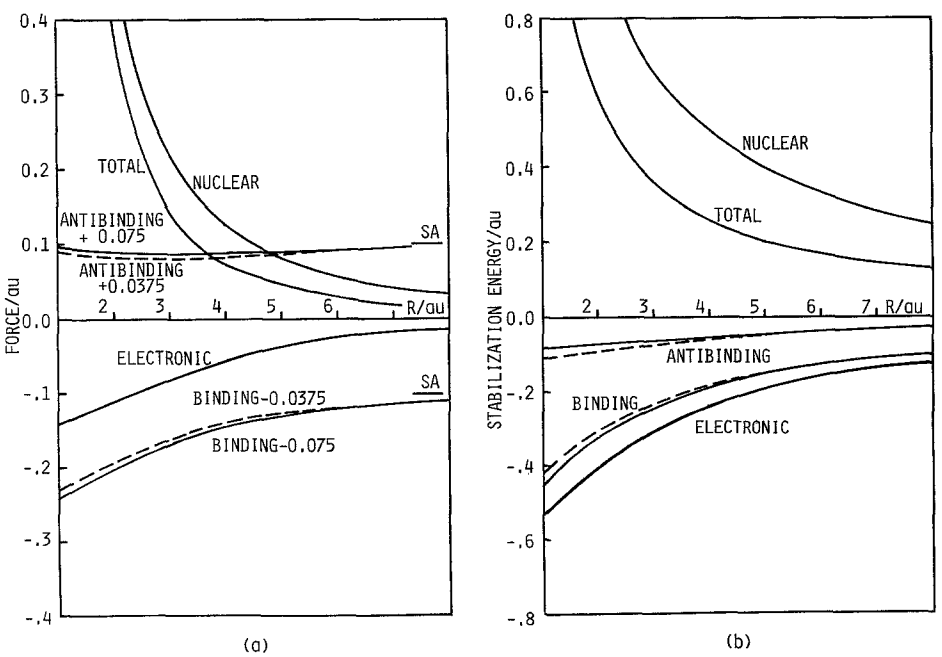

Fig. 7. $2p\pi$ State. See the captions of Fig. 2. The SA values are now $\mp 0.025/\mp 0.0625$a.u. (CMN/GCN) for the binding and antibinding forces

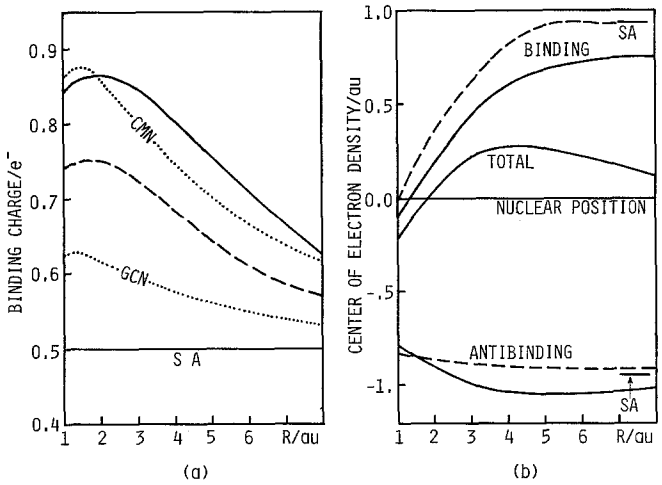

Fig. 8. $2p\pi$ State. See the captions of Fig. 3. The SA values are now 0.0 and $\pm 15/16$a.u. for the CED's

of H_2^+ system [11]: the binding and antibinding parts are cooperative for the attraction and the former contributes dominantly. Then the repulsive total force is ascribed to the smaller density preceding and the larger nuclear repulsion as has been in the $1s\sigma$ state.

Corresponding to the attractive electronic part, the density reorganizations given in Fig. 8 show a pattern of the electron-cloud preceding; the increase of the binding charge and the inward shifts of the CED's. However, the delocalization of the present π density is smaller than that of H_2^+ system. The maximum value of the net binding charge is $0.06/0.13e^-$ (CMN/GCN) in this state, while it is $0.18e^-$ in the $2p\pi_u$ state. Similarly, the maximum shift (0.28a.u.) of the total CED should be compared with that (1.3a.u.) of the $2p\pi_u$ [11].

The present results for HeH^{2+} system suggest the following: If the electron relevant to the bond formation belongs initially to heavier atom in a few-electron cationic system, atoms with very different nuclear charges are unlike to form stable molecule, since the electron density remains tightly bound by the heavier nucleus, resulting a small increase of the binding charge. This is consistent with the fact that the $1s\sigma$ states of the one-electron heteronuclear diatomics are unstable. (The energies at many internuclear distances were reported in Ref. [13] for $HeH^{2+}-OH^{8+}$.) For neutral systems, the electron density around the lighter nucleus will also suffer little effect if the heavier nucleus is almost completely shielded by its own electrons. From the region-functional viewpoint of the electron density, it is said that in stable molecules there should be some definite increase of the binding charge (and the resultant binding force) in order to counterbalance not only the antibinding contribution but also the nuclear repulsion. Within the orbital theory, this seems to give a clue for the "density interpretation" of the well-known result of the orbital

interaction theory (see e.g., [17]) that the larger the energy difference of orbitals, the smaller the mixing of the orbitals. Indeed, the $1s\sigma$ state in HeH^{2+} seems rather indifferent to the bonding like the inner shells (core orbitals) in many-electron molecules.

5. Summary

In this study, we have quantitatively examined the regional contribution of electron density for the heteronuclear HeH^{2+} system. The effect of the coordinate-dependence of the Berlin diagram has been shown to be small. The results of the two different (CMN and GCN) regional partitionings have been almost parallel.

For all the $1s\sigma$, $2p\sigma$, and $2p\pi$ states, electron-cloud preceding which accelerates the bond formation has been observed. It has appeared as the increase of the binding charge and the inward shift of the CED. However, stable bond is found only in the $2p\sigma$ state. Whether the electron density relevant to the bond formation is tightly or loosely bound by nucleus seems to be the origin of this difference. The repulsive $1s\sigma$ and $2p\pi$ states correlate with 1s(He) and $2p\pi$(He), respectively, while the attractive $2p\sigma$ state with 1s(H) in the separated atom limit. The larger nuclear charge interrupts the density flow from the antibinding to the binding region resulting a smaller density preceding and hence a smaller attraction. This has been discussed in some detail by comparing the density reorganizations in the attractive and repulsive states of HeH^{2+} and H_2^+ systems.

Acknowledgment. We thank Mr. T. Nishijima for his computational assistance. We also express our appreciation to the Data Processing Center of Muroran Institute of Technology for the use of COSMO 700 II computer. Part of this study has been supported by a Grant-in-Aid for Scientific Research from the Ministry of Education of Japan.

References

1. Berlin, T.: J. Chem. Phys. **19,** 208 (1951)
2. Hellmann, H.: Einführung in die Quantenchemie, Vienna: Deuticke, 1937; Feynman, R. P.: Phys. Rev. **56,** 340 (1939)
3. Deb, B. M.: Rev. Mod. Phys. **45,** 22 (1973)
4. Deb, B. M. ed.: The force concept in chemistry, New York: Van Nostrand Reinhold, in press
5. Koga, T., Nakatsuji, H., Yonezawa, T.: J. Am. Chem. Soc. **100,** 7522 (1978)
6. Nakatsuji, H., Kanayama, S., Harada, S., Yonezawa, T.: J. Am. Chem. Soc. **100,** 7528 (1978)
7. Nakatsuji, H.: J. Am. Chem. Soc. **95,** 2084 (1973); **96,** 24, 30 (1974); Nakatsuji, H., Koga, T.: Chapter 4 of Ref. 4
8. Nakatsuji, H., Koga, T.: J. Am. Chem. Soc. **96,** 6000 (1974)
9. Bader, R. F. W.: J. Am. Chem. Soc. **86,** 5070 (1964); Bader, R. F. W., Preston, H. J. T.: Can. J. Chem. **44,** 1131 (1966); Johnson, O.: Chem. Scr. **6,** 202, 208 (1974)
10. Bader, R. F. W., Henneker, W. H., Cade, P. E.: J. Chem. Phys. **46,** 3341 (1967) and the succeeding papers; Ransil, B. J., Sinai, J. J.: J. Chem. Phys. **46,** 4050 (1967)
11. Koga, T., Nishijima, T., Morita, M.: Theoret. Chim. Acta. (Berl.) **55,** 133 (1980).

12. Bates, D. R., Carson, T. R.: Proc. Roy. Soc. London, **A234,** 207 (1956)
13. Ponomarev, L. I., Puzynina, T. P.: 1966 JINR-P4-3175 preprint, Joint Inst. Nuclear Research, Dubna. SC-T-67-0935, Sandia Labs., Albuquerque, New Mexico
14. Winter, T. G., Duncan, M. D., Lane, N. F.: J. Phys. **B10,** 285 (1977)
15. Feinberg, M. J., Ruedenberg, K.: J. Chem. Phys. **55,** 5804 (1971)
16. Politzer, P., Harris, R. R.: J. Am. Chem. Soc. **92,** 6451 (1970); Politzer, P., Reggio, P. H.: J. Am. Chem. Soc. **94,** 8308 (1972)
17. Fukui, K.: Theory of orientation and stereoselection, Berlin: Springer-Verlag, 1975
18. Koga, T., Nakatsuji, H., Yonezawa, T.: Mol. Phys. **39,** 239 (1980)

Received February 4, 1980